

CTMRG study of the critical behavior of an interacting-dimer model

C Chatelain

Université de Lorraine, CNRS, LPCT, F-54000 Nancy, France

E-mail: christophe.chatelain@univ-lorraine.fr

Abstract. The critical behavior of a dimer model with an interaction favoring parallel dimers in each plaquette of the square lattice is studied numerically by means of the Corner Transfer Matrix Renormalization Group algorithm. The critical exponents are known to depend on the chemical potential of vacancies, or monomers. At large average density of the latter, the phase transition becomes of first-order. We compute the scaling dimensions of both order parameter and temperature in the second order regime and compare them with the conjecture that the critical behavior is the same as the Ashkin-Teller model on its self-dual critical line.

1. Introduction

Besides their experimental realizations, in particular as diatomic molecules adsorbed on a surface [1, 2], dimer models, are, with the Ising model and its generalizations, among the most studied toy models of Statistical Physics. They are also encountered in the ground state of other models, for instance the fully-frustrated Ising model on a triangular or square lattice [3] or in Resonant Valence Bond states of quantum spin-1/2 antiferromagnets [4, 5]. In the close-packed limit, the number of coverings of a 2D lattice by dimers has been computed exactly by Temperley, Fisher, and Kasteleyn [6, 7, 8]. Due to the intrinsic geometric frustration of the model, the entropy per site is non-zero and dimer-dimer correlation functions decay algebraically as $1/r^2$ with the distance r . When two lattice sites are left empty or, equivalently, when they are occupied by a monomer, the number of possible dimer configurations decay algebraically with the distance r separating the monomers as $1/\sqrt{r}$ [9, 10]. The case of a non-zero density of monomers has also been considered. The density can be either fixed or controlled by a chemical potential μ_1 . It has been shown that this monomer-dimer model does not undergo any temperature or density-driven phase transition [11, 12].

Nevertheless, a phase transition can be observed when an interaction is introduced between neighboring dimers. The case of an interaction favoring parallel dimers in a plaquette of the square lattice has been studied in detail [13, 14, 15, 16, 17]. In the close-packed limit, Monte Carlo simulations showed that the system undergoes a Berezinskii-Kosterlitz-Thouless (BKT) phase transition at $T_{\text{BKT}} = 0.65(1)$ between a low-temperature columnar ordered phase and the critical dimer phase at high temperature (Fig. 1). For a finite monomer chemical potential $\mu_1 < \mu_1^*$, and therefore a non-zero monomer density, the system undergoes a continuous phase transition with critical exponents varying with μ_1 . Transfer matrix estimates of the four smallest scaling dimensions by the gap-exponent relation support a Coulomb gas picture which implies that the interacting-dimer model shares the same critical behavior as the isotropic Ashkin-Teller model along its self-dual line. Thanks to a mapping of the latter onto the 8-vertex model, its critical exponents have been shown to be [18, 19, 20]

$$x_\sigma = \frac{1}{8}, \quad x_{\sigma\tau} = \frac{1}{8-4y}, \quad y_t = \frac{3-2y}{2-y} \quad (1)$$

where the parameter y is in the range $[0; 3/2]$ for the Ashkin-Teller model. The model is equivalent to the 4-state Potts model when $y = 0$ and to two decoupled Ising models when $y = 1$. The interacting-dimer model in the close-packed limit $\mu_1 \rightarrow -\infty$ has been conjectured to correspond to $y = 3/2$. For $0 \leq y \leq 3/2$, the scaling dimension of the dimer operator coupled by the interaction is given by $x_{\sigma\tau}$. At the monomer chemical potential μ_1^* , corresponding to $y = 0$, the phase transition becomes first-order, as predicted by mean-field theory [21]. Like the interacting-dimer model, a mixture of hard squares and dimers have been shown to undergo a phase transition that belongs to the Ashkin-Teller universality class [22]. The cases of anisotropic dimer interactions

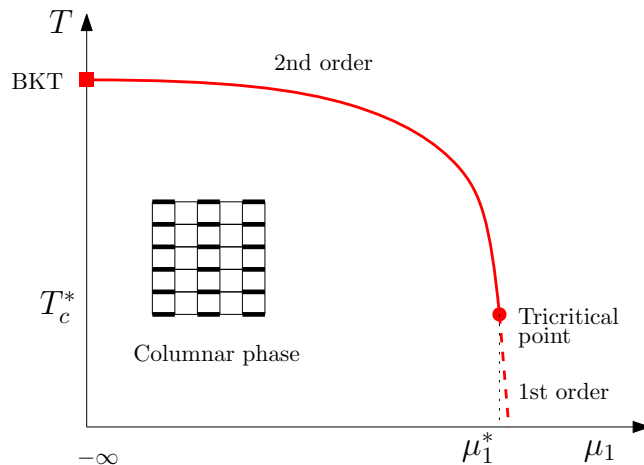


Figure 1. Schematic phase diagram of the monomer-dimer model with an interaction between parallel dimers in a plaquette (figure inspired by Fig. 1 of Ref. [14]). The close-packed limit, corresponding to the limit $\mu_1 \rightarrow -\infty$, is represented on the y -axis. T_c^* and μ_1^* are respectively the temperature and the monomer chemical potential at the tricritical point.

and repulsive interactions have been considered by transfer matrix calculations [23, 24]. On a cubic lattice, Monte Carlo simulations showed that the transition is continuous only in presence of competing plaquette and cubic interactions and a tricritical point \ddagger is also observed [25].

In the last decade, various numerical Tensor Network (TN) algorithms for the interacting-dimer model have been considered as an alternative to Monte Carlo simulations and transfer matrices. TN calculations are expected to converge faster than Monte Carlo simulations, even with worm algorithm, and to give access to much larger lattice sizes than transfer matrices. However, TN techniques are also known to be efficient only for gapped systems, i.e. away from any critical point. The unavoidable truncation of the tensors induces systematic deviations close to critical points that are difficult to estimate. It is therefore useful to test different TN algorithms and different data analysis methods to estimate critical exponents. Li *et al.* studied the interacting-dimer model by contracting the TN using an infinite time evolving block decimation (iTEBD) algorithm [15] and confirmed the phase diagram of Ref. [14]. The algebraic decay of correlation functions has been reproduced by Tensor Renormalization Group [16]. Recently, the Ashkin-Teller universality class has been tested by both TN methods and Monte Carlo simulations [17]. In this paper, we present a study of the interacting-dimer model by means of a particular TN algorithm, the Corner Transfer Matrix Renormalization Group (CTMRG) [26, 27, 28]. The latter is an extension of the celebrated Density Matrix Renormalization Group (DMRG) algorithm [29, 30] to classical statistical-mechanics models. It has been applied to a variety of lattice spin systems: Ising model in the hy-

\ddagger The word *tricritical* is used here to denote the end of the transition line of second order. Since more than 3 phases are in coexistence at the first-order phase transition, the word *multicritical* would be more rigorous.

perbolic plane [31, 32], clock model [33, 34, 35], chiral Ashkin-Teller model [36], vertex model [37] but also hard squares [38] and hard rods [39]. The CTMRG algorithm is also used to contract infinite Projected Entanglement-Pair States (iPEPS) that provide an efficient representation of 2D quantum states [40, 41].

The plan of this paper is the following: the model and the algorithm are detailed in the first section. Our estimates of the transition temperatures are presented in section 3 and compared with those obtained in Ref. [14] by transfer matrix calculations. In section 4, the order-parameter and temperature scaling dimensions are computed along the transition line in the regime of second-order phase transition. The location of the tricritical point is inferred and the conjecture of an Ashkin-Teller universality class is tested. Conclusions follow.

2. Model and CTMRG algorithm

2.1. The interacting-dimer model

We consider a square lattice $\Lambda = (E, V)$ where V denotes the set of vertices of the lattice and $E \subseteq V \times V$ the set of edges between nearest neighboring vertices. Dimers occupy edges of the lattice Λ and are not allowed to overlap, i.e. if the edge (i, j) is occupied by a dimer, no dimer can be found on the edges (i, k) and (k, j) of E . In the following, we introduce a variable $n_{ij} = n_{ji}$ equal to 1 if a dimer is present on the edge (i, j) and 0 otherwise. The vertices that are not covered by any dimer are considered to be occupied by a monomer. The variable n_i is set to 1 if a monomer is present on the vertex i and 0 otherwise. Note that the n_i 's are not independent variables: $n_i = \prod_k (1 - n_{ik})$ where the product extends over the neighbors k of the vertex i .

The average density of monomers is fixed by a chemical potential μ_1 . The presence of a monomer is therefore affected by a statistical weight $z = e^{\beta\mu_1}$ where $\beta = 1/k_B T$ ($k_B = 1$) is the inverse temperature. In addition, an interaction is introduced to favor the presence of dimers on two parallel edges of the same plaquette. The Boltzmann weight of a dimer configuration $\{n_{ij}\}$ is finally

$$W(n_{ij}) = e^{-\beta[uH + \mu_1 N_1]} \quad (2)$$

where

$$N_1 = \sum_i n_i \quad (3)$$

is the number of monomers and

$$H = \sum_{(i_1, i_2, i_3, i_4) \in \square} [n_{i_1 i_2} n_{i_3 i_4} + n_{i_1 i_3} n_{i_2 i_4}] \quad (4)$$

is the interaction energy. The symbol $\square \subseteq V^{\times 4}$ denotes the set of plaquettes of the lattice that are formed by the edges $\{i_1, i_2, i_3, i_4\}$ with (i_1, i_2) and (i_3, i_4) being horizontal edges while (i_1, i_3) and (i_2, i_4) being vertical ones. In the following, the coupling

constant u will be chosen equal to 1, without loss of generality.

Numerical calculations have shown that the low temperature phase is a columnar phase where dimers are all in the same direction, either horizontal or vertical, in every second columns or lines [13, 14]. The ground state is therefore four-fold degenerated and breaks two \mathbb{Z}_2 symmetries: the rotation of the lattice by 90° and the discrete translation by one lattice step. These two symmetries are simultaneously broken at the phase transition. Since TN algorithms are more efficient away from critical points, we introduced a small field breaking the rotational symmetry in two different ways. First, we considered a small dimer chemical potential $\Delta\mu$ with an opposite sign for horizontal and vertical dimers:

$$W(n_{ij}) = e^{-\beta[uH + \Delta\mu N + \mu_1 N_1]} \quad (5)$$

where

$$N = \sum_{(i,j) \in E_H} n_{ij} - \sum_{(i,j) \in E_V} n_{ij} \quad (6)$$

is the difference between the number of horizontal dimers and the number of vertical dimers. We also considered a small shift of the interaction coupling u with different signs for plaquettes with parallel horizontal dimers and with vertical ones:

$$W(n_{ij}) = e^{-\beta[uH + \Delta u P + \mu_1 N_1]} \quad (7)$$

where

$$P = \sum_{(i_1, i_2, i_3, i_4) \in \square} [n_{i_1 i_2} n_{i_3 i_4} - n_{i_1 i_3} n_{i_2 i_4}] \quad (8)$$

is the difference between the number of plaquettes with two horizontal dimers and the number of plaquettes with two vertical ones. The quantities P and N are not equivalent, but both break the same symmetry. Even though it is not obvious that they have the same scaling dimension, it will be shown in the following that it is indeed the case. They will therefore provide two independent estimates of the critical exponents.

2.2. CTMRG algorithm for the dimer model

To be able to use the Corner Transfer Matrix Renormalization Group (CTMRG) algorithm, the interacting-dimer model was first reformulated. Any monomer-dimer configuration $\{n_{ij}\}$ can be uniquely characterized by a set of indices $s_i \in \{0, 1, 2, 3, 4\}$ defined on the vertices of the lattice Λ . An example of such a possible one-to-one map is shown on Fig. 3. The monomer-dimer configuration of Fig. 2 for instance is encoded in the indices s_i of Fig. 4. The indices s_i always lead to a monomer-dimer configuration satisfying the constraint that two dimers cannot overlap. However, the indices s_i are not independent variables and should satisfy some compatibility constraints. In particular, if a dimer is present on the edge (i, j) then s_i and s_j should be equal to either 1 and 3 or 2 and 4, depending on the orientation of the edge. We consider then the square lattice

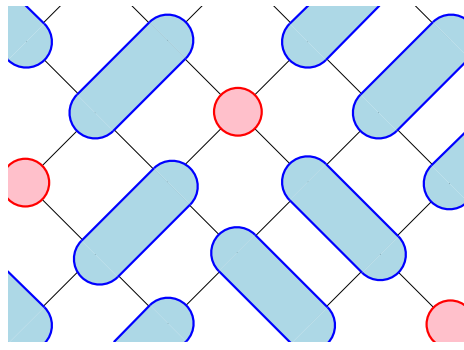


Figure 2. Example of a monomer-dimer configuration on the square lattice. Monomers are represented as red circles centered on lattice sites while dimers, in blue, overlap edges.

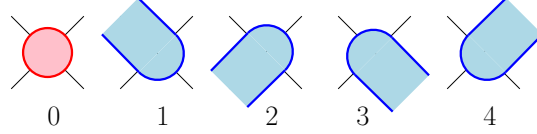


Figure 3. Indices associated to the five possible states of the system on a vertex of the lattice.

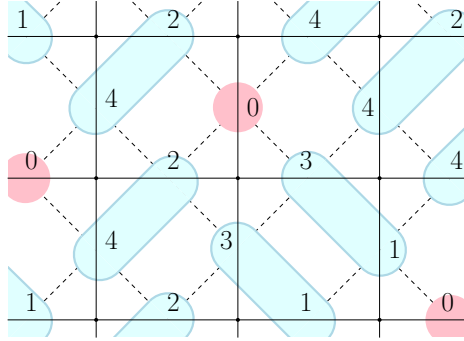


Figure 4. Vertex indices s_i corresponding to the monomer-dimer configuration of Fig. 2. The original lattice Λ is represented as dashed lines and the new lattice $\tilde{\Lambda}$ as continuous lines.

$\tilde{\Lambda} = (\tilde{V}, \tilde{E})$, at 45° of the original one, for which the vertices V of Λ lay at the center of the edges \tilde{E} of $\tilde{\Lambda}$. The indices $\{s_i\}$ are therefore carried by the edges of $\tilde{\Lambda}$. One can show that the statistical weights Eq. 2, 5, and 7 can be decomposed into a product of tensors:

$$W(s_i) = \prod_{\alpha \in \tilde{V}} \prod_{i,j,k,l \in \tilde{E}_\alpha} w_{s_i s_j s_k s_l}. \quad (9)$$

A tensor w of rank 4 is found at each vertex $\alpha \in \tilde{V}$ of the lattice $\tilde{\Lambda}$. The set $\tilde{E}_\alpha \subset \tilde{E}$ is the subset of the edges connected to the vertex α . From the indices s_i, s_j, s_k and s_l ,

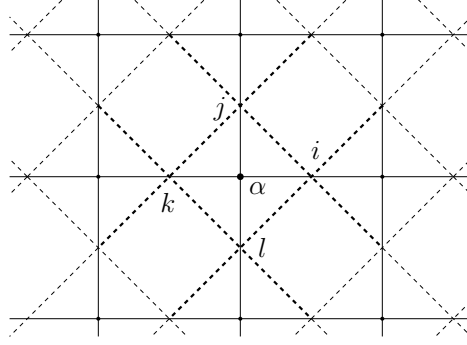


Figure 5. As in Fig. 4, the original lattice Λ is represented as dashed lines and the new lattice $\tilde{\Lambda}$ as continuous lines. A four-rank tensor $w_{s_i s_j s_k s_l}$ is placed at each vertex of $\tilde{\Lambda}$. For the vertex α (black disk at the center of the figure), the four indices s_i, s_j, s_k and s_l are located on the four nearest sites i, j, k and l of Λ . The index s_i (resp. s_j, s_k and s_l) encodes the monomer-dimer configuration on the four edges of Λ linked to i (resp. j, k and l). The knowledge of s_i, s_j, s_k and s_l allows to reconstruct the dimer occupancy of the 12 edges of Λ represented by bold dashed lines on the figure.

one can reconstruct the occupancy by a monomer on the 4 vertices i, j, k , and l of the original lattice Λ that are located around α , and the occupancy by a dimer on 12 edges (see Fig. 5). Therefore, the indices s_i, s_j, s_k and s_l give complete information on the presence of aligned dimers, either horizontal or vertical, on these 12 edges around α .

Since each index can take 5 values, the tensor w has 5^4 entries. However, most of them should always be equal to zero to impose the compatibility constraints between the indices s_i, s_j, s_k, s_l . Our tensor decomposition is different from the one introduced by Baxter for the monomer-dimer problem [42]. Baxter's tensors have only 2^4 entries but do not contain any information on the presence of aligned dimers in a given plaquette and therefore cannot be used to describe interacting dimers. Our tensors are more lightweight than the one employed in Ref. [15] which have 7^4 entries, compared to 5^4 for ours. Since the CTMRG algorithm involves Singular-Value Decompositions, we expect a smaller error with our formulation after the truncation to the same number of Singular Values. The tensors of Ref. [17] have 5^4 entries too but they lay on the original lattice Λ . Our decomposition involves therefore fewer tensors for the same number of sites.

The system is studied numerically by means of the CTMRG algorithm [26, 27, 28]. The partition function of the system is decomposed into a product

$$\mathcal{Z} = \sum_{s_1, s_2, s_3, s_4} w_{s_1 s_2 s_3 s_4} \text{Tr} [T_1^{s_1} C_1 T_2^{s_2} C_2 T_3^{s_3} C_3 T_4^{s_4} C_4] \quad (10)$$

where the T_i^s are the four Transfer matrices with a boundary degree of freedom s and the C_i are the four Corner Transfer matrices (Fig. 6). Averages of local observables are estimated as

$$\langle O \rangle = \frac{1}{\mathcal{Z}} \sum_{s_1, s_2, s_3, s_4} w_{s_1 s_2 s_3 s_4} O_{s_1 s_2 s_3 s_4}$$

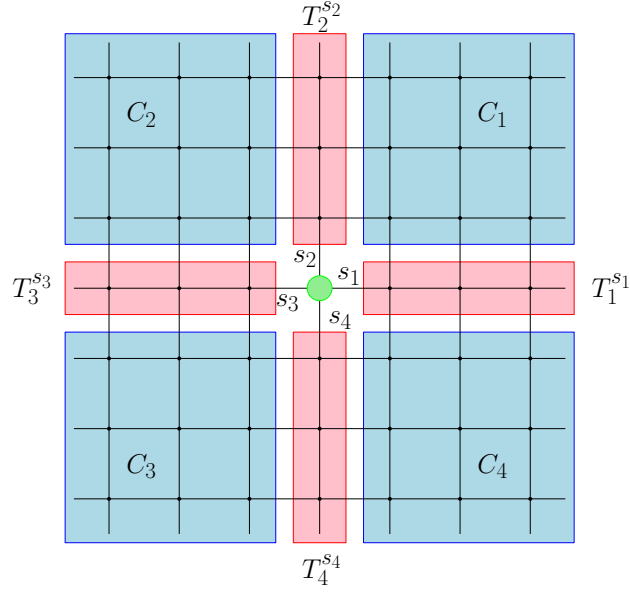


Figure 6. Decomposition of the partition function of a 7×7 system into a central vertex (green), four Transfer matrices (red) and four Corner Transfer matrices (blue). The indices of the various matrices are the indices s_i introduced above. They are on the edges of $\tilde{\Lambda}$ which are represented as continuous lines on the figure.

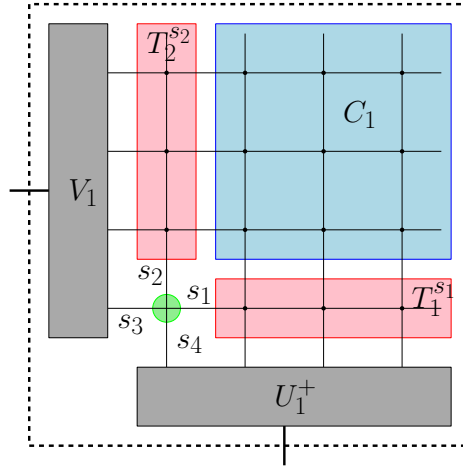


Figure 7. Extension and renormalization of the Corner Transfer matrix C_1 . The matrices U_1 and V_1 are rectangular matrices obtained from the truncation of the unitary matrices that decompose the extended Corner Transfer matrix into singular values.

$$\times \text{Tr} [T_1^{s_1} C_1 T_2^{s_2} C_2 T_3^{s_3} C_3 T_4^{s_4} C_4]. \quad (11)$$

The algorithm starts with a 3×3 system with Free Boundary Conditions. Each one of the four matrices T_i^s and C_i is attached to one site of the lattice $\tilde{\Lambda}$. After imposing the Boundary Conditions, their matrix elements are given by contractions of the tensor w , for example

$$[T_2^{s_4}]_{s_1, s_3} = \sum_{s_2} w_{s_1 s_2 s_3 s_4}, \quad [C_1]_{s_4, s_3} = \sum_{s_1, s_2} w_{s_1 s_2 s_3 s_4}. \quad (12)$$

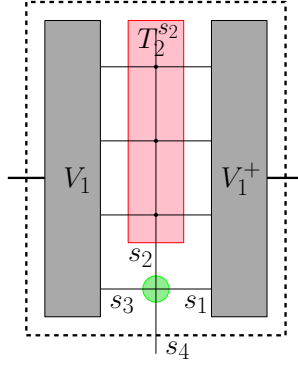


Figure 8. Extension and renormalization of the Transfer matrix T_2 .

The order of the indices of w corresponds to the convention shown on Fig. 5. The first step of the CTMRG algorithm consists in the extension of the four Corner Transfer matrices and Transfer matrices by the addition of a new vertex as depicted on Fig. 7 and 8. For the Transfer matrix, the extension reads

$$[T_2'^{s4}]_{(s_1 s_5), (s_3 s_6)} = \sum_{s_2} w_{s_1 s_2 s_3 s_4} [T_2^{s2}]_{s_5, s_6}, \quad (13)$$

while for the Corner Transfer matrix

$$[C_1']_{(s_4 s_5), (s_3 s_6)} = \sum_{s_1, s_2, s_7, s_8} w_{s_1 s_2 s_3 s_4} [T_1^{s1}]_{s_5, s_7} [C_1]_{s_7 s_8} [T_2^{s2}]_{s_8, s_6}. \quad (14)$$

In these two expressions, the notation $(s_1 s_2)$ means that the indices s_1 and s_2 are combined to form a single index. In our representation of the interacting-dimer model, the indices s_1 and s_2 take initially 5 different values, which implies that $(s_1 s_2)$ takes 25 values. At each iteration of the CTMRG algorithm, the dimension of the vector space on which act the matrices C_i and T_i is multiplied by a factor of 5. This exponential growth limits the calculation to small lattice sizes. To circumvent this limitation, a Singular Value Decomposition (SVD) of the four extended Corner Transfer matrices C_i' is performed:

$$C_i' = U_i \Lambda_i V_i^+ \quad (15)$$

where U_i and V_i are unitary matrices and Λ_i is a diagonal matrix whose elements are the singular values. The Lapack library was used to perform this SVD. The unitary matrices U_i and V_i are then truncated to a fixed number of states χ to keep only the χ largest singular values. The change of basis is applied to all matrices. The new Corner Transfer matrices

$$C_i'' = U_i^+ C_i' V_i \quad (16)$$

are now $\chi \times \chi$ diagonal matrices whose elements are the largest singular values Λ_i . This procedure, assimilated to a renormalization step, minimizes the quadratic error, defined as the Hilbert-Schmidt norm, between the original Corner Transfer matrix and its truncated version. The change of basis has to be applied to Transfer matrices too

but differently according to what they are used for. For the Transfer matrices used to compute the partition function Eq. 10, the change of basis is

$$[T_1'']^{s_1} = V_4^+ [T_1']^{s_1} U_1 \quad (17)$$

while for the Transfer matrices applied to the left (resp. right) of the Corner Transfer matrices during their extension Eq. 14

$$[T_1^{L''}]^{s_1} = U_1^+ [T_1^{L'}]^{s_1} U_1, \quad [T_2^{R''}]^{s_2} = V_1^+ [T_2^{R'}]^{s_2} V_1. \quad (18)$$

In section 3, preliminary calculations are performed with $\chi = 25$ to approximatively localize the transition line. Further calculations are then performed with $\chi = 125$ states to improve the location of the transition line. In section 4, the critical exponents will be estimated from computations with $\chi = 125$. Note that the truncation of the matrices introduces systematic deviations of the thermodynamic averages. In principle, finite Transfer matrices and Corner Transfer matrices cannot describe a critical system but only gapped systems with a finite correlation length. In the following, we will consider only the neighborhood of the transition line and not the critical line itself.

3. Phase diagram

A first series of CTMRG calculations has been performed to determine the phase diagram of the interacting-dimer model. As discussed above, the number of states kept during the truncation of the Corner Transfer matrices is limited in this section to $\chi = 25$. Thirteen monomer chemical potentials have been considered ($\mu_1 = -10, -2, -1, -0.4, 0, 0.16, 0.26, 0.28, 0.30, 0.32, 0.34, 0.36$ and 0.38) and 116 temperatures. In the last part of this section, additional calculations with $\chi = 125$ states, giving more accurate estimates of the critical temperatures, are presented.

3.1. Order parameters

As explained in subsection 2.1, a field is introduced to break the rotational symmetry of the model, either by considering a different chemical potential $\pm\Delta\mu$ for horizontal and vertical dimers or by changing the interaction to $u \pm \Delta u$ for plaquettes with respectively horizontal and vertical aligned dimers. The corresponding Boltzmann weights are given by Eqs. 5 and 7. The linear responses to these symmetry-breaking fields are order parameters of the transition: $N = \langle (n_h - n_v) \rangle$ where n_h and n_v are the densities of respectively horizontal and vertical dimers on the central vertex and $P = \langle (p_h - p_v) \rangle$ where p_h and p_v are the numbers of plaquettes with horizontal and vertical dimers on the central vertex. On Fig. 9, the order parameter N is plotted versus the temperature T for a monomer chemical potential $\mu_1 = 0$. The same curve is obtained for P . For both order parameters, the same results are obtained with a shift Δu of plaquette interaction with horizontal or vertical dimers rather than a dimer chemical potential $\Delta\mu$. As the monomer chemical potential μ_1 is increased, the transition becomes steeper and steeper and the transition temperature decreases.

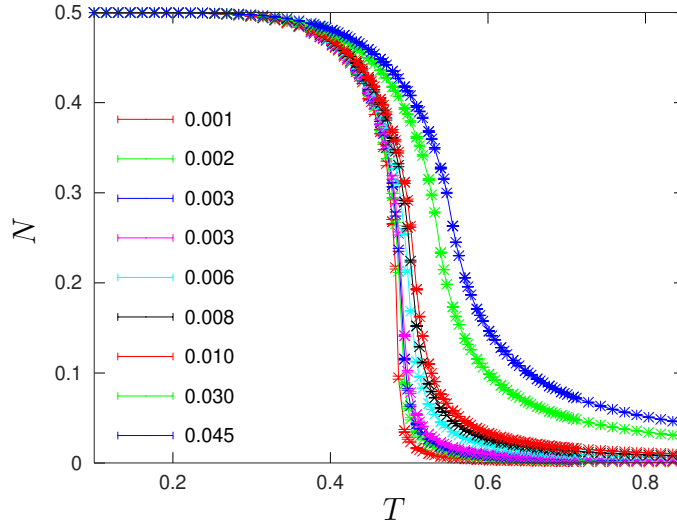


Figure 9. Order parameter N versus temperature for a monomer chemical potential $\mu_1 = 0$. The different curves correspond to different chemical potentials $\pm\Delta\mu$ of respectively horizontal and vertical dimers (0.045 is the curve at the top and 0.001 is at the bottom). The legend gives the values of $\Delta\mu$. The data have been computed with $\chi = 25$ states.

3.2. Local entropy

The entropy S_{loc} on the central vertex is easily computed in a CTMRG simulation and gives some information on the nature of the low-temperature phase. The probability distribution on the central vertex is computed as

$$\wp(s_1, s_2, s_3, s_4) = \frac{1}{\mathcal{Z}} w_{s_1 s_2 s_3 s_4} \text{Tr} [T_1^{s_1} C_1 T_2^{s_2} C_2 T_3^{s_3} C_3 T_4^{s_4} C_4] \quad (19)$$

and leads to the statistical entropy

$$S_{\text{loc}} = - \sum_{s_1, s_2, s_3, s_4} \wp \ln \wp. \quad (20)$$

We emphasize that this local entropy is not the total entropy of the system. A partial trace over the degrees of freedom described in an effective way by the Transfer matrices and the Corner Transfer matrices has been performed. The entropy associated to these degrees of freedom is therefore lost and S_{loc} is only a lower bound of the total entropy of the system. S_{loc} can be viewed as the classical analogue of the quantum entanglement entropy of the central vertex with the rest of the system. As can be seen on Fig. 10 in the case of a monomer chemical potential $\mu_1 = 0$, the local entropy is nicely compatible with the value $S = \ln 4 \simeq 1.387$ in the limit of zero temperature when no symmetry-breaking field is applied and with $S = \ln 2 \simeq 0.693$ when a different chemical potential $\pm\Delta\mu$ is assigned to horizontal and vertical dimers. The same is also observed for a different interaction strength Δu and for all considered values of the monomer chemical potential μ_1 . These values of the local entropy are consistent with the fact that the ground state of the interacting-dimer model is four-fold degenerated. The dimer chemical potentials

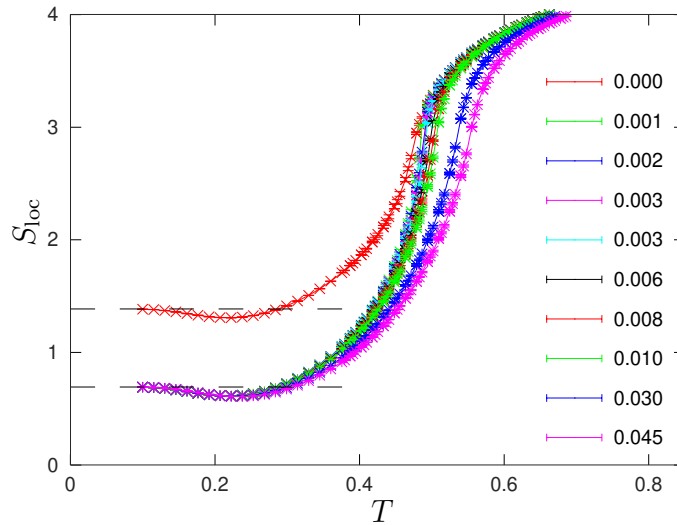


Figure 10. Statistical entropy S on the central vertex versus temperature for a monomer chemical potential $\mu_1 = 0$. The different curves correspond to different chemical potentials $\pm\Delta\mu$ of respectively horizontal and vertical dimers. The values of $\Delta\mu$ are given in the legend. The red crosses correspond to $\Delta\mu = 0$ while the other points correspond to positive symmetry-breaking fields $\Delta\mu$. The dashed lines correspond to the constant values $\ln 4$ and $\ln 2$. The data have been computed with $\chi = 25$ states.

$\pm\Delta\mu$ break rotational symmetry and therefore, reduce the degeneracy of the ground state to 2. Note that fixing the four indices s_1 , s_2 , s_3 , and s_4 determines completely the ground state. The environment of the central vertex has no additional degeneracy in the ground state. As a consequence, the local entropy is equal to the total entropy of the system at zero temperature.

3.3. Ratio of the two largest singular values

To estimate the transition temperatures, we studied the quantity

$$g = \ln \frac{\Lambda_1}{\Lambda_2} \quad (21)$$

where $\Lambda_1 \geq \Lambda_2$ are the two largest singular values of the Corner Transfer matrix. For the Ising model under a magnetic field h , the two largest singular values tend toward the same value in the limit $h \rightarrow 0$ for all temperatures $T \leq T_c$. The vanishing of g in the ferromagnetic phase is a consequence of the existence of a \mathbb{Z}_2 symmetry when $h = 0$. The vanishing of g is also observed in the ferromagnetic phase of the q -state clock model for both $q \leq 4$ and $q > 4$. In contrast, in the interacting-dimer model, g is non-zero in both the high and low-temperature phases. Instead, a dip is observed (Fig. 11). This is surprising since we have seen that the entropy takes the expected value $\ln 4$ in the limit $\Delta\mu \rightarrow 0$ (or $\Delta u \rightarrow 0$), which means that the tensor product encodes correctly the four-fold degeneracy of the ground-state. We note that the entanglement entropy of the 7-mers model has also been observed to display an unexpected behavior at the

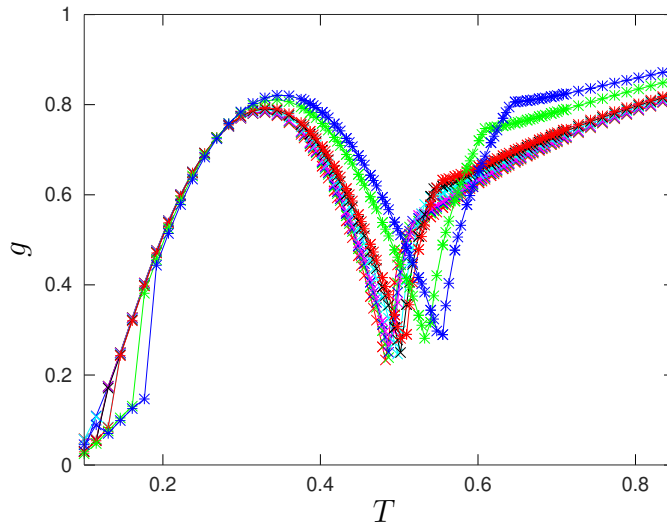


Figure 11. Logarithm of the ratio of the two largest singular values of the Corner Transfer matrix (Eq. 21) versus temperature for a monomer chemical potential $\mu_1 = 0$. The different curves correspond to different chemical potentials $\pm\Delta\mu$ of respectively horizontal and vertical dimers. The same symbols and colors as in Fig. 9 have been used. The data have been computed with $\chi = 25$ states.

two transitions [39]. In this case, as in the case of our interacting-dimer model, the Corner Transfer matrices are not symmetric. This can easily be seen for a single vertex. Using Eq. 12, one can find several possible monomer-dimer configurations contributing to $[C_1]_{32}$ while $[C_1]_{23}$ is equal to zero since the two indices are not compatible in this order. In contrast, Corner Transfer matrices are symmetric for the Ising model and their eigenvalues are real and equal to their singular values. This difference may explain the different behavior of g .

The location of the dip depends on the value of the symmetry-breaking field, either $\Delta\mu$ or Δu . It is also more rounded for negative monomer chemical potentials μ_1 and steeper for large positive ones. To improve the accuracy, we made additional calculations with $\chi = 125$ states (see Fig. 12). The temperatures of the dips, have been determined by dichotomy up to an accuracy of 10^{-5} for each monomer chemical potential μ_1 and each symmetry-breaking field $\Delta\mu$ and Δu . In the following, these temperatures are termed as pseudo-critical temperatures $T_c(\Delta\mu)$ and $T_c(\Delta u)$. We make the conjecture that the critical temperatures of the model are given by the limit of $T_c(\Delta\mu)$ (resp. $T_c(\Delta u)$) when $\Delta\mu$ (resp. Δu) goes to zero. We also expect the following scaling behavior

$$|T_c - T_c(\Delta\mu)| \sim \Delta\mu^{y_t/y_h} \quad (22)$$

where y_t is the temperature scaling dimension and y_h the scaling dimension of the order parameter N . The same scaling relation is expected for $|T_c - T_c(u)|$. As will be shown in Section 4, the two order parameters N and P share the same scaling dimension. Numerically, a non-linear fit of the data according to the law Eq. 22 turned out to be too unstable. We therefore limited ourselves to estimate the critical temperature T_c by a quadratic fit of the inverse temperature with the symmetry-breaking field. As can be

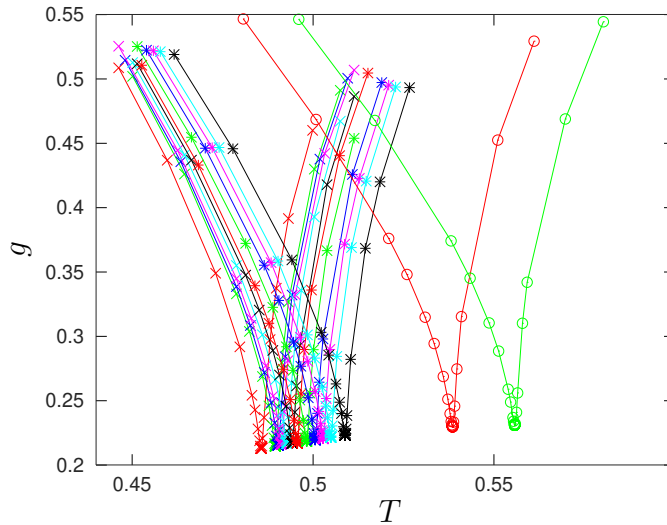


Figure 12. Logarithm of the ratio of the two largest singular values of the Corner Transfer matrix (Eq. 21) versus temperature for a monomer chemical potential $\mu_1 = 0$ with $\chi = 125$ states. The different curves correspond to different chemical potentials $\pm\Delta\mu$ of respectively horizontal and vertical dimers. $\Delta\mu = 0.001$ for the dip on the left and 0.045 for the one on the right.

noticed on Fig. 13, the fit is good for large chemical potentials μ_1 but not for $\mu_1 = -10$ or -2 . Our final estimates of the critical temperatures are presented on Fig. 14. For large chemical potentials, they are in good agreement with the transition temperatures given in Table II of Ref. [14]. This agreement provides an *a-posteriori* justification for the conjecture that the dip of g is located at the transition point. For negative monomer chemical potentials, the agreement is not so good because of the difficulty to fit properly $T_c(\Delta\mu)$ or $T_c(\Delta u)$ as mentioned above.

4. Critical behavior

In this section, the critical behavior of the interacting-dimer model along the transition line is studied. The data have been obtained with $\chi = 125$ states.

4.1. Order parameter exponent

The two order parameters N and P , defined in Sec. I, were computed at the pseudo-transition temperatures $T_c(\Delta\mu)$ and $T_c(\Delta u)$ determined as the location of the dip of g . These order parameters are expected to scale in the same way with $\Delta\mu$ and Δu :

$$N \sim \Delta\mu^{1/\delta}, \quad P \sim \Delta\mu^{1/\delta} \quad (23)$$

where $1/\delta = (d - y_h)/y_h$. The data are presented on Fig. 15 in the case of the order-parameter N . A power-law behavior is observed in an intermediate range of $\Delta\mu$ and Δu . Large $\Delta\mu$ and Δu seems to be outside the critical region where the scaling Eq. 23 holds. For small $\Delta\mu$ and Δu , one may suspect that the number of states χ kept in

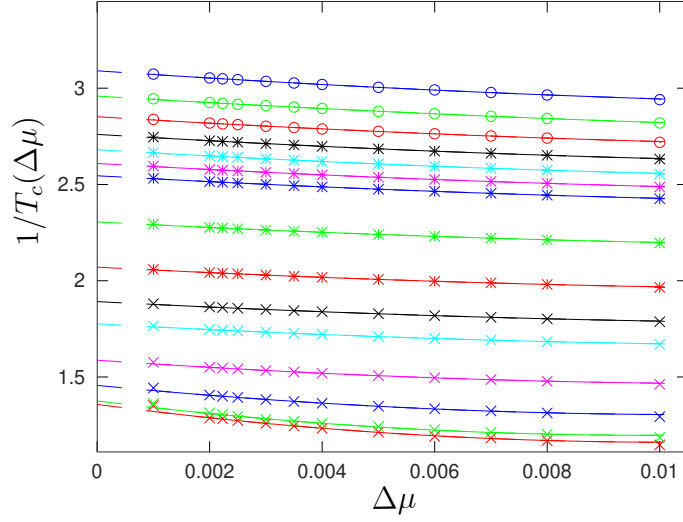


Figure 13. Inverse pseudo-transition temperatures $1/T_c(\Delta\mu)$ versus $\Delta\mu$. The different curves correspond to different monomer chemical potentials $\mu_1 = -10, -4, -2, -1, -0.4, -0.2, 0, 0.16, 0.26, 0.28, 0.30, 0.32, 0.34, 0.36$ and 0.38 (from bottom to top). The continuous curves are quadratic fits of the data.

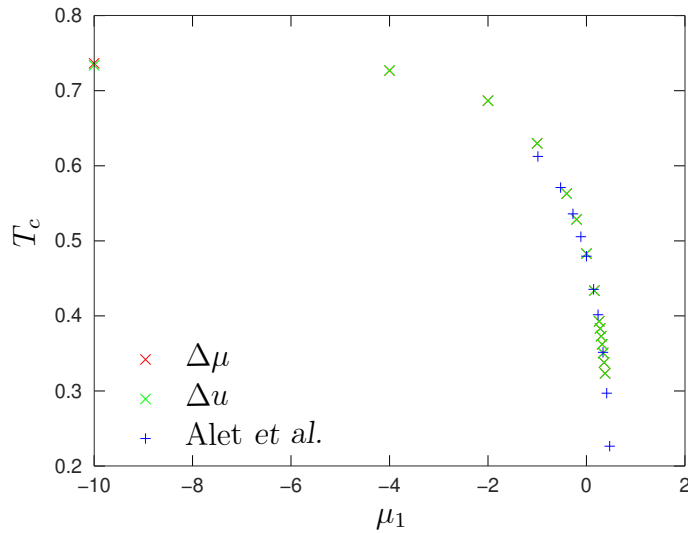


Figure 14. Extrapolated transition temperatures versus the monomer chemical potential μ_1 . The red crosses have been obtained with different chemical potentials $\pm\Delta\mu$ for horizontal and vertical dimers while the green ones with different interaction strengths Δu . The blue crosses come from Ref. [14].

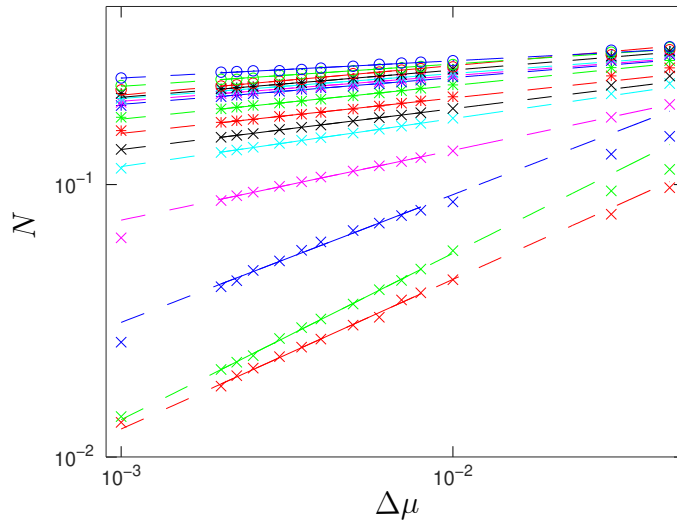


Figure 15. Order parameter N at the pseudo-transition temperatures $T_c(\Delta\mu)$ versus $\Delta\mu$. The different curves correspond to different monomer chemical potentials μ_1 . The same symbols and colors as in Fig. 12 have been used. The lines are power-law fits of the data. They are represented as continuous lines in the window where the data points have been fitted and as dashed lines outside.

the truncation of the Corner Transfer matrix becomes too small. Fig. 15 shows that the exponent $1/\delta$ clearly depends on the monomer chemical potential. On Fig. 16, the exponent $1/\delta$ is plotted versus the transition temperature T_c . The error bars represent the standard deviation of the fit. They do not take into account the error on the pseudo-transition temperatures and the systematic deviations due to the truncation of the Corner Transfer matrices. One can observe that the estimates obtained by breaking the rotational symmetry with a dimer chemical potential $\Delta\mu$ are close to those obtained with an anisotropic interaction Δu (compatible within error bars for the same order parameter) but they are systematically larger. As in Ref [14], we can estimate the temperature of the tricritical point as the temperature for which the exponent δ takes the value $\delta = 15$ of the 4-state Potts model. As can be seen on Fig. 15, our data are compatible with a monomer chemical potential $\mu_1^* \simeq 0.36$ and a transition temperature $T^* = 0.34(1)$ at the tricritical point, slightly above the estimate $0.29(2)$ of Ref [14].

4.2. Thermal critical exponent

In the process of finding the pseudo-critical temperatures $T_c(\Delta\mu)$ and $T_c(\Delta u)$, calculations were performed for at least 24 temperatures around the dip of g . These data were used to compute the temperature derivative of the order parameter. A linear fit of the two order parameters N and P with the inverse temperature $\beta = 1/k_B T$ was performed in a small window of width $\Delta\beta = 3.10^{-4}$ around the pseudo-critical temperatures $T_c(\Delta\mu)$ and $T_c(\Delta u)$. The slope of these fits gives an estimate of the

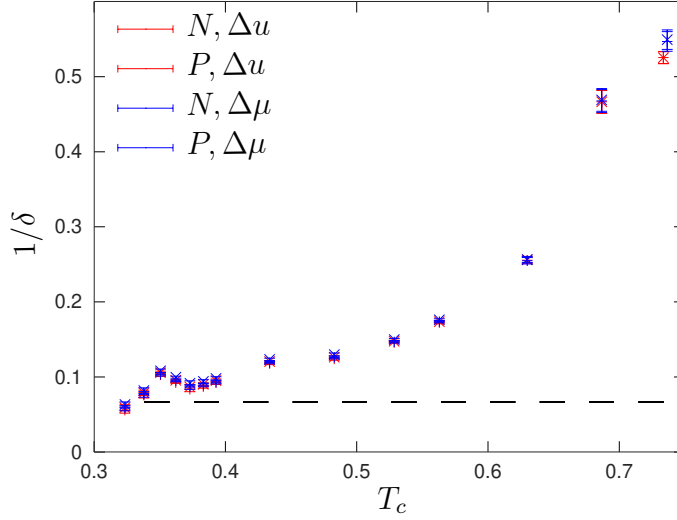


Figure 16. Exponent $1/\delta$ versus the transition temperature for the interacting-dimer model. The four sets of data points correspond to the order-parameter (N for the symbols \times and P for $+$) from which the exponent was extracted and to the field ($\Delta\mu$ in red or Δu in blue) that were introduced to break the symmetry. The dashed line is the expected value $\delta = 15$ for the 4-state Potts model.

derivatives $\frac{d}{d\beta}N$ and $\frac{d}{d\beta}P$, from which we then constructed the derivative of the logarithm

$$\frac{d}{d\beta} \ln N = \frac{1}{N} \frac{dN}{d\beta} \quad (24)$$

that is expected to scale with the symmetry-breaking fields $\Delta\mu$ and Δu as

$$\frac{d}{d\beta} \ln N \sim \Delta\mu^{-\nu_h/\nu}, \quad \frac{d}{d\beta} \ln P \sim \Delta\mu^{-\nu_h/\nu} \quad (25)$$

where $\nu_h/\nu = y_t/y_h$. The data are presented on Fig. 17. Several points are noticeably outside the curve: a red cross, corresponding to a monomer chemical potential $\mu_1 = -10$, at $\Delta\mu = 7.10^{-3}$, and two pink ones, corresponding to $\mu_1 = -1$, at $\Delta\mu = 4.10^{-3}$ and 8.10^{-3} . These points are due to the fact that sometimes the CTMRG does not find the true ground state but is trapped in excited states. A step of order $\mathcal{O}(10^{-3})$ is observed in the curve of the order parameter versus temperature when the ground state is eventually found. Because of these steps, our procedure of fitting the curve to estimate the derivative gives inaccurate estimates of $\frac{d}{d\beta}N$. The latter then lead to a critical exponent that is completely different from what is suggested by the rest of the curve and may even be negative as can be observed on Fig. 17 in the case of the red crosses and the red line. We did not try to remove these points manually so a few critical exponents are wrong and do not follow the general tendency.

Our final estimates of the critical exponents y_t/y_h are presented on Fig. 18 versus the transition temperature T_c . The figures 16 and 18 do not permit to test the conjecture that the critical behavior is the same as the Ashkin-Teller model because the relation between the critical temperatures $T_c(\mu_1)$ and the parameter y is not known. To remove the dependency on T_c , we therefore plotted y_h , extracted from $1/\delta$, versus y_t/y_h on

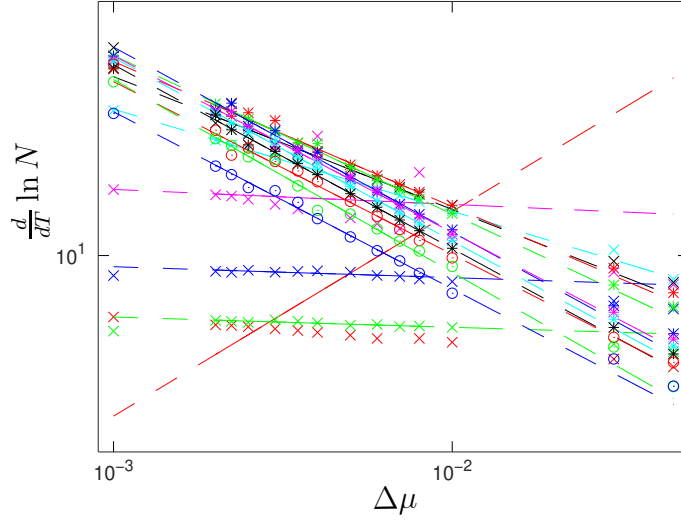


Figure 17. Derivative $\frac{d}{dT} \ln N$ of the logarithm of the order parameter at the pseudo-transition temperatures $T_c(\Delta\mu)$ versus $\Delta\mu$. The different curves correspond to different monomer chemical potentials μ_1 . The same symbols and colors as in Fig. 12 have been used. The lines are power-law fits of the data. They are represented as continuous lines in the window where the data points have been fitted and as dashed lines outside.

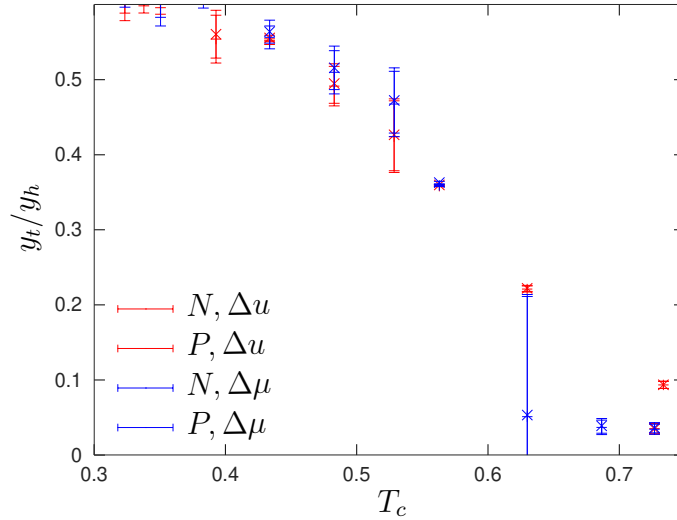


Figure 18. Exponent $1/\nu_h$ versus the transition temperature for the interacting-dimer model. The four sets of data points correspond to the order-parameter (N for the symbols \times and P for $+$) from which the exponent was extracted and to the fields ($\Delta\mu$ in red or Δu in blue) that were introduced to break the symmetry.

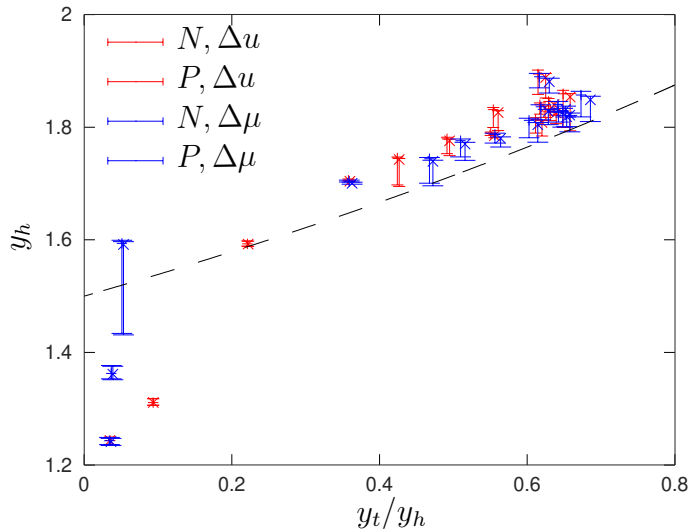


Figure 19. Scaling dimension y_h versus y_t/y_h . The four set of data points corresponds to the order-parameter (N for the symbols \times and P for $+$) from which the exponent was extracted and to the fields ($\Delta\mu$ in red or Δu in blue) that were introduced to break the symmetry.

Fig 19. For comparison, the values given by the Ashkin-Teller exponents Eq. 1 are plotted on the same figure as a dashed line from $y = 0$ (tricritical point) to $y = 3/2$ (limit $\mu_1 \rightarrow -\infty$). Apart from a few points coming from incorrect estimates of the derivatives and easily recognized by the fact that they correspond to only one of the four estimates (obtained either from N or P and with a symmetry-breaking field $\Delta\mu$ or Δu), our estimates of the scaling dimensions follow the expected trend, even though they are systematically slightly above the curve.

5. Conclusions

The scaling dimensions of the interacting-dimer model are in agreement with the conjecture that the critical behavior is the same as the Ashkin-Teller model. This confirms the ability of the CTMRG algorithm to tackle models with frustration close to their critical point. The technique has of course numerous limitations. In contrast to Monte Carlo simulations, only local observables were considered in this study of the interacting-dimer model. Even though the computation of non-local observables, as correlation functions, are possible in principle, it requires extra computations. In the case of the interacting-dimer model, we have seen that local observables are sufficient to extract the scaling dimensions y_h and y_t that define completely the critical behavior of the model. As in all tensor-network algorithms, the accuracy of the CTMRG is limited by the fact that the truncation of Corner Transfer matrices induces systematic deviations in the data. We have seen that this limitation can be circumvented, for the interacting-dimer model, by considering only non-critical points of the phase diagram. This limitation should also be put in perspective with the limitation to very small

lattices sizes in transfer matrix calculations and with the critical slowing down that plagues Monte Carlo simulations in the critical region. Finally, one should mention that the choice of the particular tensor decomposition of the partition function plays an important role in the convergence of the CTMRG algorithm. We indeed started this work with a different decomposition but were unable to reach convergence. It seems that it is important that the unit cell that is repeated in the ground state, be fully encoded in the central vertex.

Acknowledgments

This work was supported by the french ANR-PRME UNIOOPEN grant (ANR-22-CE30-0004-01). The numerical simulations were performed at the meso-center eXplor of the universit  de Lorraine under the project 2018M4XXX0118.

6. Bibliography

- [1] Fowler R H, and Rushbrooke G S, *An Attempt to Extend the Statistical Theory of Perfect Solutions*, Trans. Faraday Soc. **33**, 1272 (1937).
- [2] Roberts J K, *Some Properties of Mobile and Immobile Adsorbed Films*, Math. Proc. Camb. Phil. Soc. **34**, 399 (1938).
- [3] Nienhuis B., Hilhorst H.J. and Blote H.W.J., *Triangular SOS models and cubic-crystal shapes*, J. Phys. A: Math. Gen. **17**, 3559 (1984).
- [4] Anderson P W, *Resonating Valence Bonds: A New Kind of Insulator?*, Materials Research Bulletin **8**, 153 (1973).
- [5] Lacroix C, Mendels P, and Mila F, *Introduction to Frustrated Magnetism*, Springer Series in Solid-State Sciences.
- [6] Temperley H N V, and Fisher M E, *Dimer problem in statistical mechanics - an exact result*. The Philosophical Magazine: A Journal of Theoretical Experimental and Applied Physics **68**, 1061 (1961).
- [7] Fisher M E, *Statistical Mechanics of Dimers on a Plane Lattice*, Phys. Rev. **124**, 1664 (1961).
- [8] Kasteleyn P W, *The Statistics of Dimers on a Lattice: I. The Number of Dimer Arrangements on a Quadratic Lattice*, Physica **27**, 1209 (1961).
- [9] Fisher M E, and Stephenson J, *Statistical Mechanics of Dimers on a Plane Lattice. II. Dimer Correlations and Monomers*, Phys. Rev. **132**, 1411 (1963).
- [10] Hartwig R E, *Monomer Pair Correlations*, Journal of Mathematical Physics **7**, 286 (1966).
- [11] Heilmann O J, and Lieb E H, *Monomers and Dimers*, Phys. Rev. Lett. **24**, 1412 (1970).
- [12] Heilmann O J, and Lieb E H, *Theory of Monomer-Dimer Systems*, Commun.Math. Phys. **25**, 190 (1972).
- [13] Alet F, Jacobsen J L, Misguich G, Pasquier V, Mila F, and Troyer M, *Interacting Classical Dimers on the Square Lattice*, Phys. Rev. Lett. **94**, 235702 (2005).
- [14] Alet F, Ikhlef Y, Jacobsen J L, Misguich G, and Pasquier V, *Classical Dimers with Aligning Interactions on the Square Lattice*, Phys. Rev. E **74**, 041124 (2006).
- [15] Li S, Li W, and Chen Z, *Kosterlitz-Thouless Transitions and Phase Diagrams of the Interacting Monomer-Dimer Model on a Checkerboard Lattice*, Phys. Rev. E **90**, 052104 (2014).
- [16] Roychowdhury K and Huang C Y, *Tensor Renormalization Group Approach to Classical Dimer Models*, Phys. Rev. B **91**, 205418 (2015).
- [17] Morita S, Lee H Y, Damle K, and Kawashima N, *Ashkin-Teller Phase Transition and Multicritical Behavior in a Classical Monomer-Dimer Model*, Phys. Rev. Research **5**, 043061 (2023).

- [18] Kadanoff L P, *Connections between the Critical Behavior of the Planar Model and That of the Eight-Vertex Model*, Phys. Rev. Lett. **39**, 903 (1977).
- [19] Nienhuis B, *Critical Behavior of Two-Dimensional Spin Models and Charge Asymmetry in the Coulomb Gas*, J Stat Phys **34**, 731 (1984).
- [20] Baxter R J, *Exactly solved models of statistical mechanics*, Academic Press, Londres (1982)
- [21] Alberici D, Contucci P, and Mingione E, *The Exact Solution of a Mean-Field Monomer-Dimer Model with Attractive Potential*, EPL **106**, 10001 (2014).
- [22] Ramola K, Damle K, and Dhar D, *Columnar Order and Ashkin-Teller Criticality in Mixtures of Hard Squares and Dimers*, Phys. Rev. Lett. **114**, 190601 (2015).
- [23] Otsuka H, *Classical Dimer Model with Anisotropic Interactions on the Square Lattice*, Phys. Rev. E **80**, 011140 (2009).
- [24] Otsuka H, *Phase Transitions in Square-Lattice Dimer Model with Anisotropic Interactions*, Computer Physics Communications **182**, 1888 (2011).
- [25] Charrier D, and Alet F, *Phase Diagram of an Extended Classical Dimer Model*, Phys. Rev. B **82**, 014429 (2010).
- [26] Nishino T, *Density matrix Renormalization Group Method for 2d Classical Models*, J. Phys. Soc. Jpn. **64**, 3598 (1995).
- [27] Nishino T and Okunishi K, *Corner Transfer matrix Renormalization Group Method*, J. Phys. Soc. Jpn. **65**, 891 (1996),
- [28] Nishino T and Okunishi K, *Corner Transfer matrix Algorithm for Classical Renormalization Group*, J. Phys. Soc. Jpn. **66**, 3040 (1997)
- [29] White S R, *Density matrix Formulation for Quantum Renormalization Groups*, Phys. Rev. Lett. **69**, 2863 (1992).
- [30] White S R, *Density-matrix Algorithms for Quantum Renormalization Groups*, Phys. Rev. B **48**, 10345 (1993).
- [31] Ueda K, Krcmar R, Gendiar A, and Nishino T, *Corner Transfer matrix Renormalization Group Method Applied to the Ising Model on the Hyperbolic Plane* J. Phys. Soc. Jpn. **76** 084004 (2007)
- [32] Krcmar R, Gendiar A, Ueda K, and Nishino T, *Ising model on hyperbolic lattice studied by corner transfer matrix renormalization group method*, J. Phys. A: Math. Theor. **41** 125001 (2008)
- [33] Gendiar A, Krcmar R, Ueda K, and Nishino T, *Phase transition of clock models on hyperbolic lattice studied by corner transfer matrix renormalization group method*, Phys. Rev. E **77** 041123 (2008)
- [34] Krcmar R, Gendiar A, and Nishino T, *Phase transition of the six-state clock model observed from the entanglement entropy*, Acta Physica Polonica A **137** 598 (2020)
- [35] Ueda H, Okunishi K, Harada K, Krcmar R, Gendiar A, Yunoki S, and Nishino T, *Finite-m Scaling Analysis of Berezinskii-Kosterlitz-Thouless Phase Transitions and Entanglement Spectrum for the Six-State Clock model*, Phys. Rev. E **101**, 062111 (2020)
- [36] Nyckees S, and Mila F, *Commensurate-Incommensurate Transition in the Chiral Ashkin-Teller Model*, Phys. Rev. Research **4**, 013093 (2022).
- [37] Ueda K, Otani R, Nishio Y, Gendiar A, and Nishino T, *Critical Point of a Symmetric Vertex Model*, J. Phys. Soc. Jpn. **74** 1871 (2005)
- [38] Nyckees S, and Mila F, *Tensor Network Investigation of the Hard-Square Model*, Phys. Rev. B **106**, 174433 (2022).
- [39] Chatelain C and Gendiar A, *Absence of logarithmic divergence of the entanglement entropies at the phase transitions of a 2D classical hard rod model*, Eur. Phys. J. B **93**, 134 (2020)
- [40] Orús R and Vidal G, *Simulation of Two-Dimensional Quantum Systems on an Infinite Lattice Revisited: Corner Transfer matrix for Tensor Contraction*, Phys. Rev. B **80**, 094403 (2009).
- [41] Cirac I, Perez-Garcia D, Schuch N, and Verstraete F, *matrix Product States and Projected Entangled Pair States: Concepts, Symmetries, and Theorems*, Rev. Mod. Phys. **93**, 045003 (2021)
- [42] Baxter R J, *Dimers on a Rectangular Lattice*, Journal of Mathematical Physics **9**, 650 (1968).